Neuro-Oncology Advance Access published October 31, 2015

Neuro-Oncology

Neuro-Oncology 2015; **0**, 1–9, doi:10.1093/neuonc/nov263

MRI contrast agent for targeting glioma: interleukin-13 labeled liposome encapsulating gadolinium-DTPA

Xiaoli Liu, Achuthamangalam B. Madhankumar, Patti A. Miller, Kari A. Duck, Susan Hafenstein, Elias Rizk, Becky Slagle-Webb, Jonas M. Sheehan, James R. Connor, and Qing X. Yang

Department of Neurosurgery, Pennsylvania State University College of Medicine, Hershey, Pennsylvania (X.L., A.B.M., K.A.D., E.R., B.S.-W., J.M.S., J.R.C., Q.X.Y.); Department of Radiology, Pennsylvania State University College of Medicine, Hershey, Pennsylvania (X.L., P.A.M., Q.X.Y.); Department of Microbiology, Pennsylvania State University College of Medicine, Hershey, Pennsylvania (S.H.)

Corresponding Author: Qing X. Yang, PhD, Department of Radiology, 500 University Drive, H066, Hershey, PA, 16802 (qyang@hmc.psu.edu).

Background. Detection of glioma with MRI contrast agent is limited to cases in which the blood-brain barrier (BBB) is compromised as contrast agents cannot cross the BBB. Thus, an early-stage infiltrating tumor is not detectable. Interleukin-13 receptor alpha 2 (IL-13Rα2), which has been shown to be overexpressed in glioma, can be used as a target moiety. We hypothesized that liposomes conjugated with IL-13 and encapsulating MRI contrast agent are capable of passing through an intact BBB and producing MRI contrast with greater sensitivity.

Methods. The targeted MRI contrast agent was created by encapsulating Magnevist (Gd-DTPA) into liposomes conjugated with IL-13 and characterized by particle size distribution, cytotoxicity, and MRI relaxivity. MR image intensity was evaluated in the brain in normal mice post injection of Gd-DTPA and IL-13-liposome-Gd-DTPA one day apart. The specificity for glioma detection by IL-13-liposome-Gd-DTPA was demonstrated in an intracranial glioma mouse model and validated histologically.

Results. The average size of IL-13-liposome-Gd-DTPA was 137 ± 43 nm with relaxivity of 4.0 ± 0.4 L/mmole-s at 7 Tesla. No significant cytotoxicity was observed with MTS assay and serum chemistry in mice. The MRI signal intensity was enhanced up to 15% post injection of IL-13-liposome-Gd-DTPA in normal brain tissue following a similar time course as that for the pituitary gland outside of the BBB. MRI enhanced by IL-13-liposome-Gd-DTPA detected small tumor masses in addition to those seen with Magnevist-enhanced MRI.

Conclusions. IL-13-liposome-Gd-DTPA is able to pass through the uncompromised BBB and detect an early stage glioma that cannot be seen with conventional contrast-enhanced MRI.

Keywords: glioma, liposome, IL-13, blood-brain barrier (BBB), targeted MRI contrast agent.

The outcome for treating malignant glioma has remained poor, with an overall median survival of 14 months after diagnosis.[1] One of the major reasons for such a dismal outcome is lack of a sensitive tool for detecting infiltrating tumors at an early stage when treatment is more effective. Currently available MRI contrast agents for the detection of brain tumors, such as gadolinium diethylenetriaminepentacetate (Gd-DTPA, Magnevist), are nonspecific and only detect tumor masses that have significantly damaged the blood-brain barrier (BBB).[2] Malignant brain tumors in their early stage, especially glioblastoma multiforme (GBM), infiltrate aggressively into the brain tissues, where they cannot be enhanced by the MRI contrast agent in most cases because the BBB has not been significantly damaged. Moreover, the borders indicated by contrast-enhanced MRI do not necessarily reflect all of the tumor and normal tissue boundaries. GBM generally recurs because of the proliferation of undetected infiltrating tumor cells or the chemoresistant glioma stem cells that migrate from the primary tumor sites. The current clinical image modalities (ie, MRI, PET, and CT) can only resolve a tumor size of ≥ 2 mm.[3,4] The effectiveness of current treatment and development of new therapies is thus critically limited by the difficulties in detection of these infiltrating tumors at an early stage distal to the primary tumor sites.

The BBB consists of astrocytes, basement membrane, and endothelial cells characterized by intercellular tight junctions that prevent 98% of small molecules and all large molecules from entering the brain. In addition, lipid-mediated molecules are restricted to diffuse in and out of the BBB if they are

Received 9 March 2015; accepted 24 September 2015

>400 Da and form >8 hydrogen bonds.[5,6] The ability to penetrate the BBB has been a challenge for developing diagnostic and therapeutic agents for tumors in the CNS.[7–9]

Liposomes have been shown to be a promising drug delivery vehicle to the CNS because of their ability to encapsulate drugs and conjugate antibodies or ligands on their surface.[10–12] Drug transport to the brain with targeted liposomes has shown improved efficacy for treating tumor animal models, indicating that liposomes have the ability to pass through the BBB.[13] However, it has not been directly demonstrated in vivo that liposomes can cross an intact BBB. Previous studies demonstrated that liposomes could deliver Gd-DTPA into hepatoma and enhance the MRI contrast.[14–17] For the purpose of detecting tumors in the brain with MRI, however, a contrast agent having the ability to pass through the BBB could present a potential problem because it would enhance all brain tissue and thus lose its ability to differentially highlight the tumor tissues. Therefore, the liposome carrying an MRI contrast agent must be able to specifically target brain tumor tissues in order to highlight them. Fortunately, it has been demonstrated that glioma tumor cells overexpress interleukin-13 receptors alpha 2 (IL-13Rα2), while cells in normal brain tissues and other organs only express insignificant amounts of IL-13Rα2.[18,19] Based on Debinski et al, 100% of high-grade gliomas (grade III) and GBMs, 60% of oligodendrogliomas, 50% of gliosarcomas, and 24% of low-grade gliomas overexpress IL-13Rα2.[20–22] According to Sikorska et al, 100% of high-grade astrocytomas overexpress IL-13Rα2.[23] In a recent review article, IL-13Rα2 was expressed in 58% of adult and 83% of pediatric brain tumors.[24] The overexpression of IL-13Rα2 on malignant glioma cells with 30 000 IL-13 binding sites per cell has created an opportunity for using liposomes to target glioma cells.[25] Utilizing this property, Madhankumar et al applied IL-13-liposomes (IL-13-Lip) containing an anticancer drug (doxorubicin) that specifically targeted the GBM and led to a more effective therapeutic outcome than utilizing doxorubicin alone.[26,27] Debinski et al also found that IL-13Rα2-targeted therapy preferentially targeted the stem-like cell population, which possibly indicated decreased tumorigenicity in vivo.[28] IL-13 was also used as a brain tumor target for imaging.[22,26] Chittiboina et al applied antibody interleukin-13–*Pseudomonas* exotoxin with the co-infusion of Gd-DTPA.[29] Based on these studies, we hypothesized that encapsulation of Magnevist into liposomes conjugated with IL-13 would generate a novel contrast agent that could cross the intact BBB and target glioma cells specifically, such that early stage glioma could be detected. To test our hypothesis, glioma U251 and glioma stem cell lines isolated from GBM patients and athymic nude mice were selected as our in-vitro and in-vivo models, respectively.[21,30,31] This report presents the development and characterization of IL-13-Lip-Gd-DTPA and provides in-vivo evidence of its ability to cross an intact BBB in normal mouse brain and its ability to target infiltrating glioma tissues in the mouse tumor model.

Materials and Methods

All animal experimental procedures were carried out in accordance with institutional guidelines and approved by the Animal Care and Use Committee of the Pennsylvania State University College of Medicine.

Preparation and Characterization of IL-13-Lip-Magnevist (IL-13-Lip-Gd-DTPA)

A lipid mixture consisting of 1,2-dipalmitoyl-*sn*-glycero-3-phosphocholine (DPPC), cholesterol, 1,2-distearoyl-*sn*-glycero-3 phosphoethanolamine-N-[carboxy(polyethylene glycol)-2000] (ammonium salt) (DSPE-PEG(2000) carboxylic acid) and 1,2-distearoyl-*sn*-glycero-3-phosphoethanolamine-N-[maleimide(polyethylene glycol)-2000] (ammonium salt) (DSPE-PEG(2000) Maleimide) in the mole ratio of 10:5:5:0.5 was dissolved in a mixture of methanol/chloroform 1:1 (volume to volume ratio). Subsequently, the organic solvent was evaporated using a rotator vapor to receive a film. With the vibration of ultrasound, the film was reconstituted in a saturated solution mixed by Gd-DTPA with poly-L-lysine (Sigma) (ratio, 8 mL:5 mg) to formulate multilamellar vesicles. The multilamellar vesicles were extruded through the polycarbonate membranes with 4 passes through at 200 and 100 nm sequentially. Then, Lip-Gd-DTPA was conjugated with human IL-13 protein by incubating the IL-13 with Lip-Gd-DTPA overnight at 4°C.[26] To remove the free IL-13 protein, the sample with IL-13-Lip-Gd-DTPA was passed through a Sepharose CL-2B column, and then IL-13-Lip-Gd-DTPA was exhaustively dialyzed overnight against PBS at 4°C and concentrated for the final product.

The size distribution of IL-13-Lip-Gd-DTPA was determined by measuring the polydispersity index with light-scattering analysis using Malvern Zetasizer (Ver. 3.16; Brookhaven Instruments). The morphology of IL-13-Lip-Gd-DTPA was examined with a negative stain transmission electron microscopy (TEM) (JEOL 1400 TEM at 120 kV). To evaluate the loading efficiency of Gd in IL-13-Lip, IL-13-Lip-Gd-DTPA was digested in 20% nitric acid overnight at 100°C, and the concentration of Gd was then quantified using inductively by coupled plasma-atomic emission spectroscopy (ICP-AES) with a Perkin Elmer spectrometer. Consistent with previous stability studies,[32] IL-13-Lip-Gd-DTPA in phosphate-buffered saline is stable at 4°C for at least one month based on its size distribution and MRI relaxivity measurements, which were performed as a quality assurance routine before all in-vivo experiments.

IL-13-Lip-Gd-DTPA Crossing the Blood-brain Barrier in an in-vitro Model

The ability of IL-13-Lip-Gd-DTPA to cross the BBB was evaluated using an established bichamber in-vitro BBB model, as previously described;[26] details can be found in the Supplementary Materials.

IL-13-Lip-Gd -DTPA Crossing the Blood-brain Barrier in a Normal Mouse in-vivo Model

MRI studies were carried out to evaluate the ability of IL-13-Lip-Gd-DTPA to penetrate an intact BBB in vivo with normal mice. Two groups of animals ($n = 3$) were anesthetized with 2% isoflurane/oxygen and subsequently injected through the tail vein with either free Magnevist or IL-13-Lip-Gd-DTPA. The amount of injection was normalized to 736 μg of gadolinium. Axial T1-weighted images were acquired on a 7.0 T MRI system with 540/11 ms TR/TE, 8 NEX, 192 × 192 matrix, 32 mm FOV, 0.5 mm slice thickness at the following time points: one preinjection and 5 postinjection scans at 30, 60,

and 120 minutes and 24 hours. The signal-to-noise ratios (SNRs), graphed as time course against SNR of preinjection and postinjection images were evaluated from 2 regions of interest: (i) the posterior pituitary gland where the BBB is absent as an internal reference and (ii) the brain parenchyma on the same image slice.

Glioma Mouse Model and Histological Chemistry

For testing IL-13-Lip-Gd-DTPA as a targeted contrast agent for glioma, the intracranial tumor model was prepared as previously described.[26,28] The tumor formation and volume were monitored weekly with Magnevist-enhanced T1-weighted MRI starting at 2 weeks post tumor induction. When a tumor reached a size of 5–10 mm in diameter, the mice were imaged with the T1-weighted scan after injection of Magnevist as a control and FITC-labeled liposome (IL-13-Lip(FITC)-Gd-DTPA). Then, the mice were euthanized at ~2 hours post injection of IL-13-Lip(FITC)-Gd-DTPA, and the brains were harvested and frozen immediately at −20°C. The brain tissue was sectioned at a 12 μm thickness at −20°C and mounted on slides. The selected neighboring brain tissue slides were stained separately with hematoxylin and eosin (H&E) for tumor tissue identification, or DAPI for FITC-labeled liposomes accumulation in the glioma or with immunostaining for observation of IL-13Rα2 differential expressions between glioma and adjacent normal tissue following the standard protocol (See details in Supplementary Materials).

A number of other tests were performed. IL-13-Lip-Gd-DTPA uptake, cytoxicity by GSC T3691 and U251, and in-vivo toxicity in mouse model were conducted. Immunoblotting analyses were performed for conjugation of IL-13 with liposomes and expression of IL-13Rα2 in glioma and glioma stem cells. An MRI study was carried out for each batch of IL-13-Lip-Gd-DTPA. The experimental procedures of the above-mentioned studies are described in detail in the Supplemental Material in the sections of animal models and cell cultures, uptake of IL-13-Lip-Gd-DTPA by GSC T3691 and U251, cytotoxicity of IL-13-Lip-Gd-DTPA, in-vivo toxicity studies, immunoblotting analysis of the conjugation of IL-13 with liposomes, immunoblotting analysis for expression of IL-13Rα2 in glioma and glioma stem cells, immunohistochemistry in normal mouse model, and MRI study of IL-13-Lip-Gd-DTPA.

Results

Characterization of IL-13-Lip-Gd-DTPA

The average size of IL-13-Lip-Gd-DTPA was 137 ± 43 nm, which was consistent for four 4°C different batches. Fig. 1A shows an example of the size distribution, with a polydispersity index of 0.1–0.2 nm indicating that the size of the liposome was uniformly produced. The TEM image in Fig. 1B provides visualization of the spherical morphology of IL-13-Lip-Gd-DTPA. The loading efficiency of gadolinium in IL-13-Lip was within the range of 4.0–10.0 mg/L determined by measuring concentration of gadolinium in IL-13-Lip-Gd-DTPA using ICP-AES. The

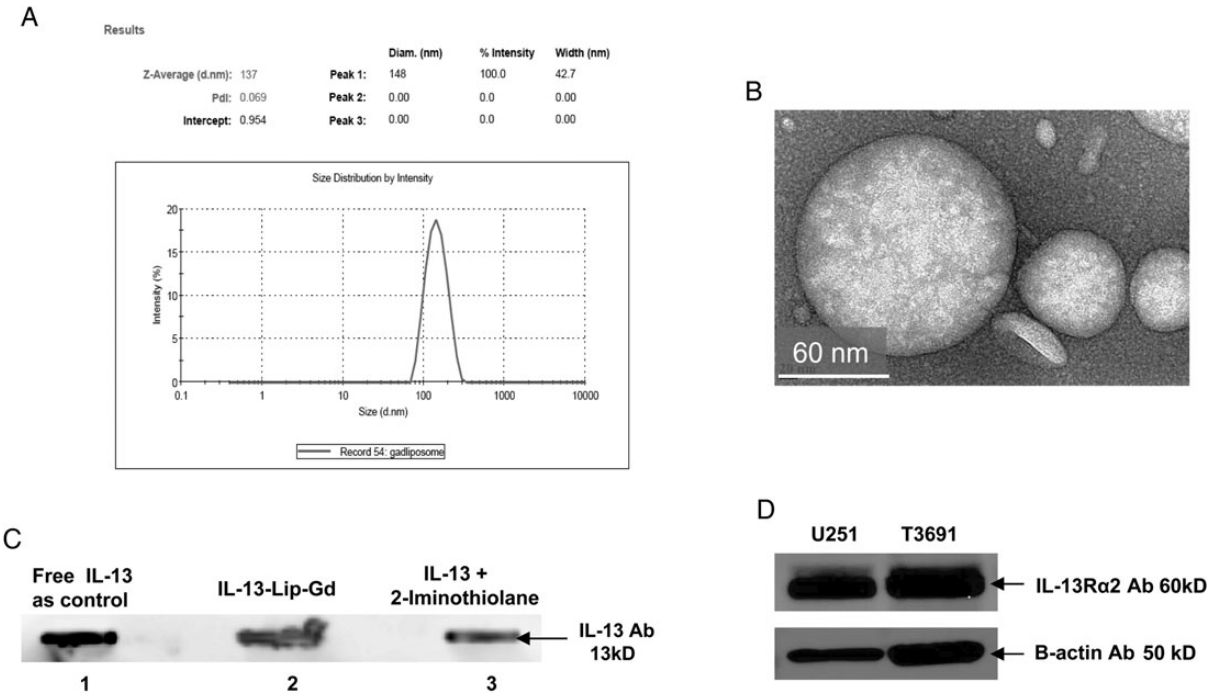

Fig. 1. Characteristics of the liposome. (A) The size (diameter) distribution of IL-13-Lip-Gd-DTPA determined by light scattering and zeta potential analyzer. The average diameter of IL-13-Lip-Gd-DTPA was 137 nm within a range of 90–180 nm. (B) An image acquired by transmission electronic microscopy demonstrated the spherical morphology of IL-13-Lip-Gd-DTPA. (C) Immune analysis of IL-13 incorporation to the liposomes. The dark band in lane 1 indicates the recombinant protein IL-13 as a control. The dark band in lane 2 (loaded with IL-13-Lip-Gd-DTPA) and in lane 3 (loaded with an intermediate product, IL-13-2-thiolation of the conjugation) indicate incorporation of IL-13 into the liposomes. (D) Western blotting analysis of U251 and T3691 cells that expressed IL-13Rα2.

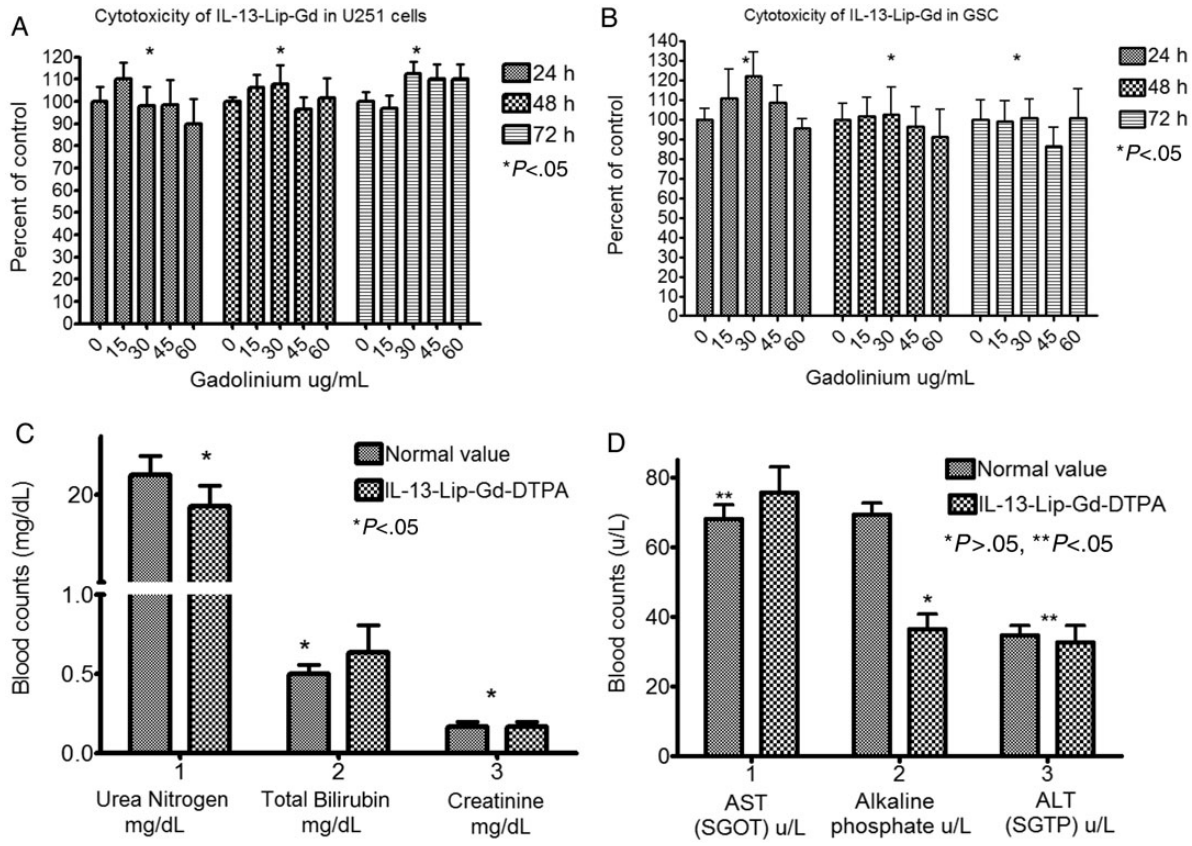

Fig. 2. Toxicity assessments of IL-13-Lip-Gd-DTPA on cell culture and blood chemistry. (A) MTS assay of U251 cells and (B) T3691 cells that were incubated with various Gd concentrations of IL-13-Lip-Gd-DTPA at 3 time points. The optical density was normalized to the controls. No significant differences were found among all concentrations of Gd from IL-13-Lip-Gd-DTPA exposed in cell proliferation ($P < .05$, ANOVA). (C, D) The graphs showed the markers of toxic index in blood chemistry compared with the untreated control mice. No significant difference was observed in 5 of the toxic markers index compared with control (*$P < .05$, Student t test) except alkaline phosphatase.

conjugation of IL-13 with the liposomes was confirmed through immunoblotting analysis as shown in Lane 2 in Fig. 1C. The dark band in lanes 1, 2, and 3 represent the original recombinant IL-13 protein, its conjugated complex with liposomes, and the intermediate species (2-Iminothiolane), respectively, indicating the existence of IL-13 in each form. The Western immunoblotting analysis shown in Fig. 1D revealed that the IL-13Rα2 Ab was overexpressed in glioma U251 and T3691 cells, as anticipated.

IL-13-Lip-Gd-DTPA Toxicity Assessment

The cytotoxicity of the liposomes was not observed in either the in-vitro MTS assay or the in-vivo serum chemistry data. As shown in Fig. 2A and B, U251 and T3691 cell exposure to Gd concentrations in liposomes from 15 μg/mL–60 μg/mL did not produce a significant difference in cell cytotoxicity when compared with the controls using MTS assays. In addition, the blood serum chemistry study between the control (injection of Magnevist) and the injection of IL-13-Lip-Gd-DTPA into mice did not show any significant toxicity in terms of blood urea nitrogen mg/dL, total bilirubin mg/dL, creatinine mg/dL (Fig. 2C), AST U/L, and ALT U/L (Fig. 2D). However, alkaline phosphatase U/L, appeared to be lowered in the mice treated with liposomes, which was likely caused by the minor perturbations of nutritional uptake.[33]

IL-13-Lip-Gd-DTPA Uptake

Figure 3 shows confocal microscopy images captured after exposure of FITC labelled IL-13-Lip-Gd-DTPA to the cell cultures. The FITC green color in Fig. 3A–C indicated the presence of liposomes in the cytosol of glioma U251, U87, and T3691 cells, respectively, thus demonstrating the uptake of IL-13-Lip-Gd-DTPA by all 3 cell lines.

IL-13-Lip-Gd-DTPA Crossing BBB in-vitro Model

Figure 4 shows the Gd concentration transported from the apical to the basal chamber of the BBB in-vitro model at 2, 4, and 24 hours. At 2 hours, the Gd concentration of free Gd-DTPA and IL-13-Lip-Gd-DTPA did not show a marked difference. But at 4 hours, the Gd concentration from the IL-13-Lip-Gd-DTPA was 6000 μg/L, which is 3-fold greater than that from free Gd-DTPA. This difference in Gd concentration in the basal chamber suggested that IL-13-Lip-Gd-DTPA facilitated Gd crossing the BBB in the in-vitro model. Rhodamine-labeled dextran,

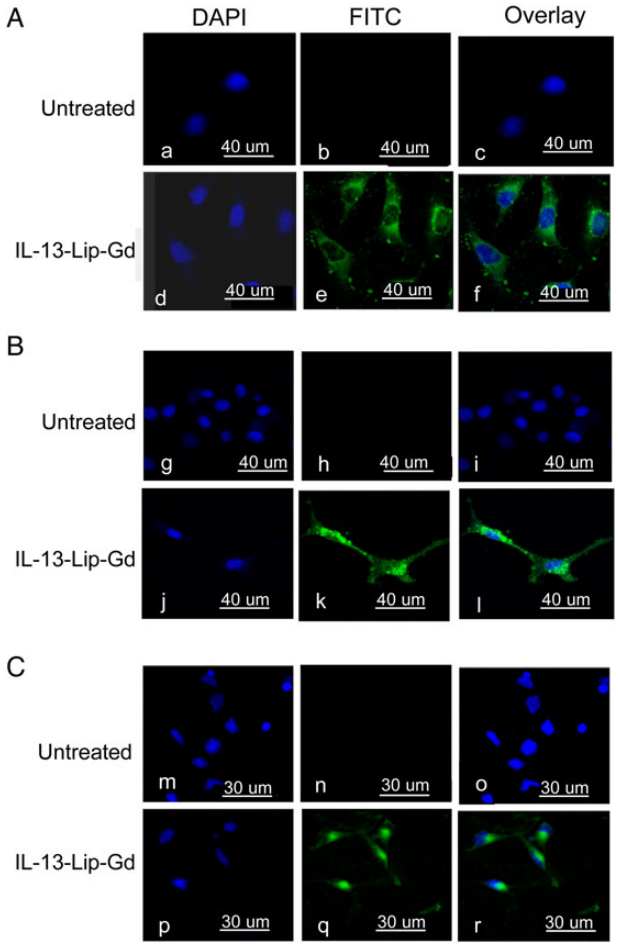

Fig. 3. Confocal microscopy images for IL-13-Lip-Gd-DTPA uptake in cell culture, (A) U251, (B) U87, and (C) T3691, respectively. Blue color indicates the nucleus stained with DAPI, and green color indicates FITC-labeled liposomes. The overlay for the 2 images in the left column shows the internalization of the FITC-labeled IL-13-Lip-Gd-DTPA in glioma tumor cell lines.

present on the apical chamber of the model, served as an indicator of the integrity of the tight junctions and was not observed in the basal chambers.[27]

IL-13-Lip-Gd-DTPA Crossing BBB in Normal Mice

The encapsulation of contrast agent into the liposomes made it possible to assess the ability of liposomes to cross the intact BBB in vivo by MRI by injection of IL-13-Lip-Gd-DTPA into normal mice. For histological analysis, the liposomes used in this study were labeled with FITC. As illustrated in Fig. 5A, the signal changes in the pituitary gland (blue trapezoid) and the brain tissues (red ellipse) were measured on the T1-weighted MRI of the same slice post injection of either Magnevist or IL-13-Lip-Gd-DTPA. The signal changes of the pituitary gland were used to make certain that the contrast agents IL-13-Lip-Gd-DTPA (Fig. 5A-a-◆) or Magnevist (Fig. 5A-c-◆) entered the blood stream. Since the pituitary gland does not have a BBB, the signal increased for about a 2 hour period in the pituitary gland for both cases, indicating that the

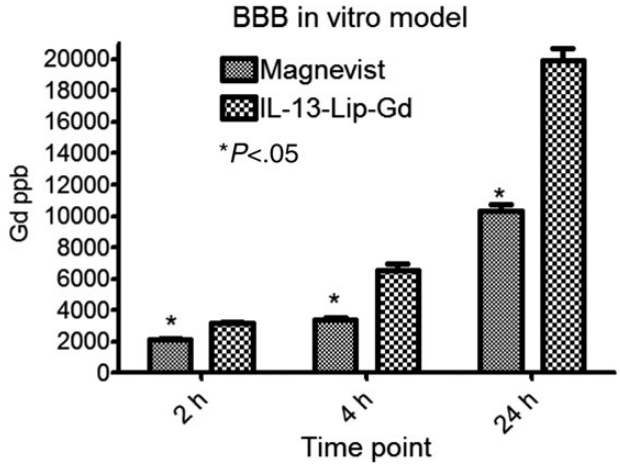

Fig. 4. Concentrations of Gd at the bottom well of the in-vitro blood-brain barrier (BBB) model at 2, 4, and 24 hour time points. The concentration of Gd is doubled at 4 and 24 hours post exposure of IL-13-Lip-Gd-DTPA compared with Magnevist. Significant differences were found for all 3 time points (*$P < .05$, Student t test).

liposomes encapsulated with Gd-DTPA were capable of inducing similar MRI contrast as Magnevist. Accordingly, the signal change in brain parenchyma provided an indication whether IL-13-Lip-Gd-DTPA or Magnevist crossed the intact BBB. As shown in the time courses in Fig. 5A-a-■, the signal of brain parenchyma followed similar temporal characteristics as that of the pituitary gland, with an increase up to 15% at 30 minutes post injection of IL-13-Lip-Gd-DTPA. As anticipated with injection of Magnevist, the signal from brain parenchyma shown in Fig. 5A-c-B remained unchanged because the Magnevist was blocked by the intact BBB. These data provided the first direct in-vivo evidence that IL-13-Lip-Gd-DTPA penetrated an intact BBB and entered the brain parenchyma of a living mouse.

To validate the in-vivo findings, histology was performed on the animals. Fig. 5B shows confocal microscopy images from a brain tissue section of a mouse after injection of FITC labeled IL-13-Lip-Gd-DTPA Fig. 5B-(a-f) and a control Fig. 5B-(g-i), respectively. The confocal images confirmed the in-vivo results with a widespread FITC distribution in the brain tissue compared with the complete absence of FITC in brain tissues without injection of IL-13-Lip(FITC)-Gd-DTPA. It is also important to note that the FITC-labeled liposomes were sparsely distributed. The magnified image (63X) in Fig. 5B-e indicated that the liposomes remaining in the brain were intracellular. The confocal microscopy images in Fig. 5C showed DAPI, FITC-liposomes, Ab GFAP-rhodamines, and co-localization of IL-13-Lip(FITC)-Gd-DTPA in a, b, c and d, respectively, which also confirmed that IL-13-Lip(FITC)-Gd-DTPA entered the brain tissue and co-localized with one of the astrocytes markers, GFAP.

Detection of Glioma by IL-13-Lip-Gd-DTPA

To further test the functionality of IL-13-Lip-Gd-DTPA as an MRI contrast agent for the detection of glioma, Fig. 6A shows an example of T1-weighted MR images acquired at the identical location from the same mouse with an intracranial tumor after

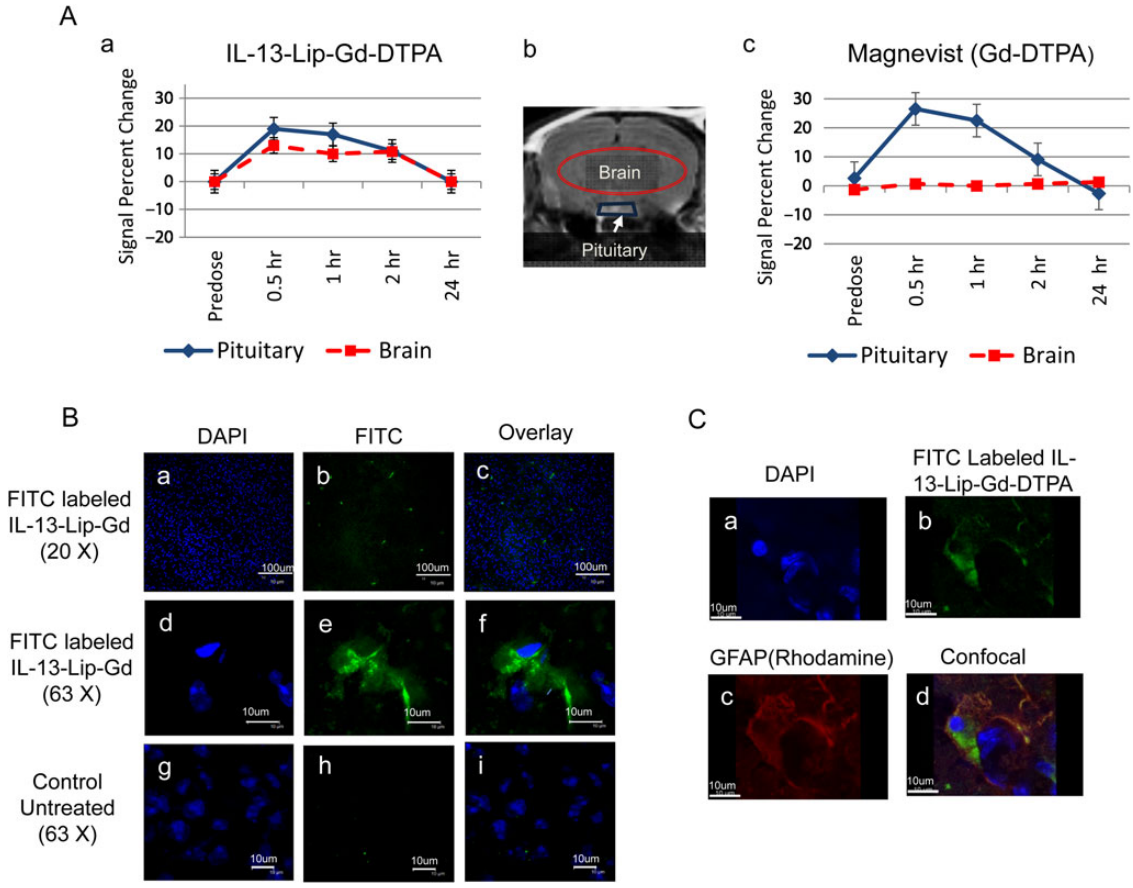

Fig. 5. (A) The plots of an average signal intensity time-course measured in T1-weighted images post injections of IL-13-Lip-Gd-DTPA (A-a) or Magnevist (A-c) into the brain parenchyma and pituitary gland shown in the brain image (A-b) in normal animals ($n = 6$). The image intensity plot in blue ◆ in the location of pituitary (indicated in blue trapezoid in the brain image in b) followed the same trend for both IL-13-Lip-Gd-DTPA and Magnevist, indicating that the injections of IL-13-Lip-Gd-DTPA and Magnevist were successful. The signal in the brain parenchyma ■ (indicated by the red-oval region in the brain image) after injection of Magnevist stays the same, while after injection of IL-13-Lip-Gd-DTPA the signal increases to about 15%. The increase in signal intensity in the brain tissue indicated that the MRI contrast agent crossed an intact blood-brain barrier (BBB) with liposomes. (B) Confocal microscopy images of brain slides. The blue color in the left column indicated the nucleus stained with DAPI (B-a, B-d, B-g), and the green color of FITC sparsely distributed in the middle column (B-b, B-e) showed the existence of IL-13-Lip in the brain tissue, confirming the penetration of the intact BBB of normal mice. The overlay for the 2 images in the right column (B-c, B-f) indicated that the retained liposomes were intracellular. No FITC was observable in the images of untreated mice (B-h, B-i). (C) Confocal microscopy images. (C-a) DAPI, (C-b) IL-13-Lip(FITC)-Gd-DTPA; (C-c) Rhodamine-labeled astrocytes marker GFAP; (C-d), co-localization of IL-13-Lip(FITC)-Gd-DTPA with GFAP in a normal brain tissue section.

receiving the Magnevist (Fig. 6A-a,-c) and IL-13-Lip-Gd-DTPA injections 24 hours apart (Fig. 6A-b, -d). As seen in the MR images from the primary tumor site, IL-13-Lip-Gd-DTPA produced similar contrast as Magnevist (white arrows) and delineated the tumor masses. However, there were additional small tumor masses that could be identified by IL-13-Lip-Gd-DTPA proximal to the primary tumor site (red arrows in Fig. 6A-b). Similarly, as indicated in Fig. 6A-d, IL-13-Lip-Gd-DTPA detected several additional tumor masses, which Magnevist failed to delineate, in the brain slice about 2 mm posterior to the primary site in Fig. 6A-c. This finding was confirmed by histology of the same tissue slice shown in Fig. 6B. As indicated in the zoomed-in image of H&E stain in Fig. 6B-e, f, a tumor mass (dark purple color) was positively identified in the same location as in the MRI image in Fig. 6A-d. In this tumor site, high accumulation of FITC-labeled liposomes were observed in Fig. 6B-g, indicating the effective targeting of the liposome. Accordingly, the confocal immunohistochemistry image in Fig. 6B-h demonstrated IL-13Rα2 differential expressions in glioma and the adjacent normal tissues.

Discussion

We presented novel in-vivo data demonstrating that we have developed a nanotechnology platform capable of passing through the BBB and delivering MRI contrast directly to brain tumors. The BBB is the major obstacle in delivering chemotherapeutic agents to the brain. Current techniques for enhancing penetration of the BBB can be classified into 2 categories: (i) bypassing the BBB through convection-enhanced delivery[34,35] and focused ultrasound-mediated delivery.[36,37] These kinds of approaches can be effective for delivering drugs to

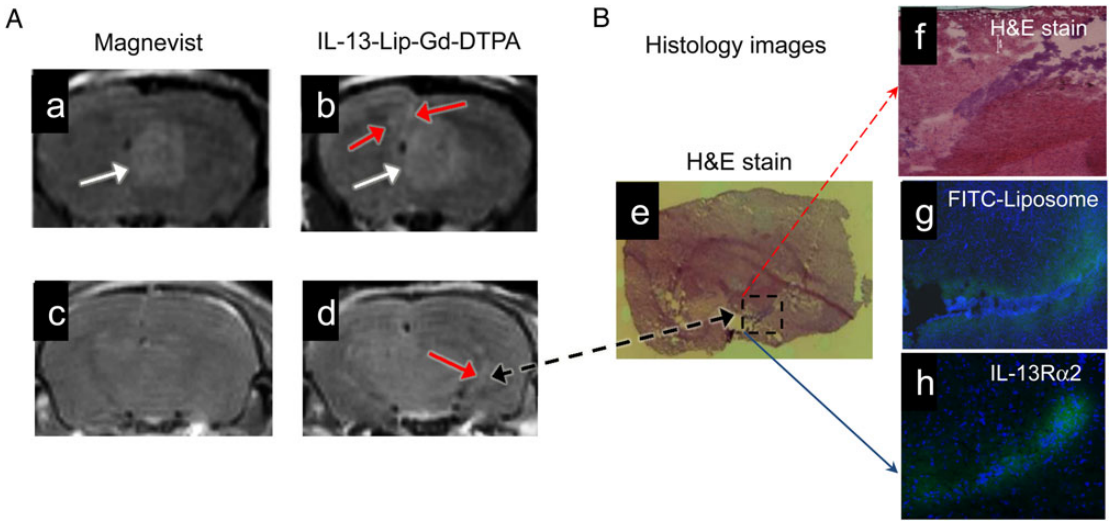

Fig. 6. (A) T1-weighted MRI of glioma enhanced with Magnevist (a, c) and IL-13-Lip-Gd-DTPA (b, d) from the same animal. The images of the same brain slice (a, b) show the primary tumor (white arrows). Additionally enhanced focal areas (red arrows) peripheral to the primary site are shown only with IL-13-Lip-Gd-DTPA. The images (c, d) were acquired from a brain slice 2 mm posterior to the primary site and show additional tumor masses (red arrow) only with liposomes. (B) Image (B-e) of histology slice within the same brain slice in MR image in A-d. Image (B-f) is zoomed into an infiltrating brain tumor (blue color) in the dashed line box in the hematoxylin and eosin (H&E) stain. The corresponding microscopy image (B-g) shows FITC-labeled liposomes (green color) focal in the tumor area. Image (B-h) shows a confocal image of immunohistochemistry overlaid with DAPI obtained from a brain slide 300 μm from the H&E image (B-e). The differential expression of IL-13Rα2 in the glioma and adjacent normal tissues is clearly demonstrated.

known cancer sites, but convection-enhanced delivery is invasive, and ultrasound-mediated delivery requires the stratum corneum to be intact and is time-consuming to administer, all of which offer little help for cancer detection. (ii) BBB nondisruptive approaches such as receptor-mediated delivery with liposomes or other delivery vehicles. Surface-pegylated liposomes are often used for this purpose because pegylation improves liposome stability in the blood stream and subsequently enhances ability to deliver agents.[38,39] Such liposomes, especially those of a smaller size (eg, 50–200 nm), are believed to be able to extravasate the relatively permeable vasculature of tumors and promote efficient accumulation in the tumor interstitium (a phenomenon known as the enhanced permeability and retention (EPR) effect). However, there had been no direct experimental evidence and method to assess such ability in vivo. By encapsulating MRI contrast agent into our liposome, the penetration of an intact BBB by the liposome is clearly indicated in vivo in normal mice. Furthermore, our liposomal approach provides a possibility for developing our nanotechnology into a theranostic delivery system by combining chemotherapeutic agents or molecular targets with the MRI contrast agent.

Previous in-vivo data demonstrating that the liposome was capable of penetrating the BBB were based on indirect measurements showing higher drug efficacy with the liposome in an intracranial tumor model.[27] Since the BBBs of the intracranial tumor models are known to be compromised, the data obtained with tumor models are deemed to be inconclusive on the ability of the liposome to cross the BBB. In our data shown in Fig. 5A-a, the MRI signal was enhanced up to 15% in the brain tissue with IL-13-Lip-Gd-DTPA in normal mice without a tumor. The MRI signal enhancement in the brain followed the same temporal characteristics as the pituitary gland, which served as an intracranial reference outside the BBB. In addition, the in-vivo data were validated histologically from the same group of mice by fluorescently labeling the FITC. A certain amount of FITC was found to be sparsely distributed in the brain tissues in all animals treated with FITC-labeled liposome as shown in Fig. 5B-b. Co-localization of FITC-labeled IL-13-Lip(FITC)-Gd-DTPA with astrocyte marker GFAP is illustrated in Fig. 5C-b,-c and Fig. 5C-d demonstrates that IL-13-Lip(FITC)-Gd-DTPA entering the normal brain tissue. Taken together, our experimental results provided concrete evidence that IL-13-liposome facilitates Gd-DTPA passing through an uncompromised BBB.

Comparing the time course from in-vitro model, our in-vivo data indicated that the in-vitro model may not be suitable for the study of the kinetics of this process as it uses only gravitational force in thermal equilibrium to increase interactions with the endothelial cell layer, while the blood flow, blood pressure, vessel geometry, and morphologies for the in-vivo condition are all involved in the liposomal transport into the BBB. In future studies, it will be necessary to acquire quantitative data on IL-13-Lip-mediated transport of gadolinium through the BBB in order to understand the underlying mechanism and establish a kinetic model.

The average size and size distribution of the liposomes are important factors for their ability to cross the BBB and for systematic cytotoxicity.[40] Thus, the size distribution and the lipid composition of the liposomes have been previously studied intensively.[14–16,41] The average size of our liposome was 130 nm distributed within a narrow range of 40–300 nm (Fig. 1). Our liposome was composed of polyethylene glycol (PEG), which permitted the liposome to escape the immune system responses and increase its circulating time.[42] With this formulation, no

detectable cytotoxicity was observed in either cell culture or serum blood chemistry.

As we discussed in the introduction, our liposome facilitates the MRI contrast agent passing through the BBB, but it is not sufficient if the contrast agent is not differentially accumulated in the tumor. As shown in the brain image of a normal mouse in Fig. 5A-a, the MRI signal from the brain parenchyma increased uniformly at the same time after injection of our IL-13-Lip-Gd-DTPA and yielded no visible image contrast change. We knew that the measurements of brain Gd-DTPA tissue concentrations using MRI and ICP-AES demonstrated a high degree of coincidence. [43] Thus, in order to highlight tumors, a contrast agent must be able to preferentially target the tissue of interest. As shown by the comparison in Fig. 6A-a and Ab, IL-13-Lip-Gd-DTPA generated similar contrast as Magnevist. In this case, both contrast agents could perfuse into the brain tissue near the tumor site where the BBB was compromised. A closer look at the images in Fig. 6A-b and -d reveals several additional enhanced areas surrounding the primary tumor site. The areas enhanced only by IL-13-Lip-Gd-DTPA were infiltrating tumors. The advantage of our targeted contrast agent is undoubtedly demonstrated in Fig. 6A-b and A-d, where the tumor masses are small, distal to the primary site, and can be identified only with our liposomal contrast agent. As seen in Fig. 6B, the infiltrating tumor identified by our contrast agent presented the typical histological characteristics of GBM. In this case, the tumor masses had not caused significant damage to the BBB such that it could not be detected with Magnevist Fig. 6A-c. The large amount of FITC found in this tumor site in Fig. 6B-g is additional confirmation that the contrast in the tumor produced by our agent was a result of its ability to pass through the BBB and preferentially deliver the MRI contrast agent to the glioma tissues. In addition, those tumor masses enhanced only by IL-13-Lip-Gd-DTPA preserved signal enhancement 24 hours post injection. The sustained signal enhancement by our targeted liposome in the infiltrating tumor sites behind the intact BBB was possible only if the contrast agent was in the intracellular space. This is consistent with the previous studies. In these studies, the targeting ability for glioma was determined indirectly by assessing its efficacy in inhibiting the tumor growth.[26]

Conclusion

We have developed and characterized IL-13-Lip-Gd-DTPA. We demonstrated in vivo that our agent is capable of delivering Gd-DTPA through the intact BBB in normal mice and preferentially targeting the glioma tissues in an intracranial mouse model. The in-vivo data were validated with postmortem histology from the same animal. The significance of this research is addressing an unmet need in diagnosis and treatment of glioma by developing a novel MRI contrast agent that directly targets specific receptors on the neoplastic cells, thereby enhancing uptake of the MRI contrast locally in the tumor tissues with greater specificity and sensitivity. Our approach provides feasibility for future development of a theranostic agent targeting glioma.

Supplementary Material

Supplementary material is available online at Neuro-Oncology (http://neuro-oncology.oxfordjournals.org/).

Funding

None declared.

Conflict of interest statement. There is no conflict of interest for any of the authors.

References

1. Reardon DA, Rich JN, Friedman HS, Bigner DD. Recent advances in the treatment of malignant astrocytoma. *J Clin Oncol*. 2006;24(8):1253–1265.
2. Nathan C, Varghai D, Flask CA, Oleinick NL, Feyes DK, Dean D. Optional Gadolinium dose level for magnetic resonance imaging (MRI) contrast enhancement of U87-derived tumors in athymic nude rats for the assessment of photodynamic therapy. *Proc of SPIE*. 2009;7161(2Y):1–10.
3. Fatterpekar GM, Galheigo D, Narayana A, Johnson G, Knopp E. Treatment-related change versus tumor recurrence in high-grade gliomas: a diagnostic conundrum–use of dynamic susceptibility contrast-enhanced (DSC) perfusion MRI. *AJR Am J Roentgenol*. 2012;198(1):19–26.
4. Vriens D, van Laarhoven HW, van Asten JJ, et al. Chemotherapy response monitoring of colorectal liver metastases by dynamic Gd-DTPA-enhanced MRI perfusion parameters and 18F-FDG PET metabolic rate. *J Nucl Med*. 2009;50(11):1777–1784.
5. Madsen SJ, Hirschberg H. Site-specific opening of the blood-brain barrier. *J Biophotonics*. 2010;3(5-6):356–367.
6. Roberts J, Kahle MP, Bix GJ. Perlecan and the blood-brain barrier: beneficial proteolysis? *Front Pharmacol*. 2012;3(155):1–5.
7. Pardridge WM. Drug transport across the blood-brain barrier. *J Cereb Blood Flow Metab*. 2012;32(11):1959–1972.
8. Pardridge WM. The blood-brain barrier: bottleneck in brain drug development. *NeuroRx*. 2005;2(1):3–14.
9. Pardridge WM. Blood-brain barrier delivery. *Drug Discov Today*. 2007;12(1–2):54–61.
10. Bangham AD, Horne RW. Negative staining of phospholipids and their structural modification by surface-active agents as observed in the electron microscope. *J Mol Biol*. 1964;8:660–668.
11. Huwyler J, Wu D, Pardridge WM. Brain drug delivery of small molecules using immunoliposomes. *Proc Natl Acad Sci USA*. 1996;93(24):14164–14169.
12. Sapra P, Allen TM. Ligand-targeted liposomal anticancer drugs. *Prog Lipid Res*. 2003;42(5):439–462.
13. Schnyder A, Huwyler J. Drug transport to brain with targeted liposomes. *NeuroRx*. 2005;2(1):99–107.
14. Tilcock C, Unger E, Cullis P, MacDougall P. Liposomal Gd-DTPA: preparation and characterization of relaxivity. *Radiology*. 1989;171(1):77–80.
15. Unger EC, MacDougall P, Cullis P, Tilcock C. Liposomal Gd-DTPA: effect of encapsulation on enhancement of hepatoma model by MRI. *Magn Reson Imaging*. 1989;7(4):417–423.
16. Unger EC, Winokur T, MacDougall P, et al. Hepatic metastases: liposomal Gd-DTPA-enhanced MR imaging. *Radiology*. 1989;171(1):81–85.
17. Vartholomeos P, Fruchard M, Ferreira A, Mavroidis C. MRI-guided nanorobotic systems for therapeutic and diagnostic applications. *Annu Rev Biomed Eng*. 2011;13:157–184.

18. Caput D, Laurent P, Kaghad M, et al. Cloning and characterization of a specific interleukin (IL)-13 binding protein structurally related to the IL-5 receptor alpha chain. *J Biol Chem*. 1996;271(28): 16921–16926.
19. Debinski W, Gibo DM. Molecular expression analysis of restrictive receptor for interleukin 13, a brain tumor-associated cancer/ testis antigen. *Mol Med*. 2000;6(5):440–449.
20. Debinski W, Gibo DM, Hulet SW, Connor JR, Gillespie GY. Receptor for interleukin 13 is a marker and therapeutic target for human high-grade gliomas. *Clin Cancer Res*. 1999;5(5):985–990.
21. Debinski W, Slagle B, Gibo DM, Powers SK, Gillespie GY. Expression of a restrictive receptor for interleukin 13 is associated with glial transformation. *J Neurooncol*. 2000;48(2):103–111.
22. Fillmore HL, Shultz MD, Henderson SC, et al. Conjugation of functionalized gadolinium metallofullerenes with IL-13 peptides for targeting and imaging glial tumors. *Nanomedicine (Lond)*. 2011;6(3):449–458.
23. Witusik-Perkowska M, Zakrzewska M, Szybka M, et al. Astrocytoma-associated antigens - IL13Ralpha2, Fra-1, and EphA2 as potential markers to monitor the status of tumour-derived cell cultures in vitro. *Cancer Cell Int*. 2014;6(3):449–458.
24. Sengupta S, Thaci B, Crawford AC, Sampath P. Interleukin-13 receptor alpha 2-targeted glioblastoma immunotherapy. *Biomed Res Int*. 2014;2014(1):1–8.
25. Debinski W, Obiri NI, Powers SK, Pastan I, Puri RK. Human glioma cells overexpress receptors for interleukin 13 and are extremely sensitive to a novel chimeric protein composed of interleukin 13 and *Pseudomonas* exotoxin. *Clin Cancer Res*. 1995;1(11):1253–1258.
26. Madhankumar AB, Slagle-Webb B, Mintz A, Sheehan JM, Connor JR. Interleukin-13 receptor-targeted nanovesicles are a potential therapy for glioblastoma multiforme. *Mol Cancer Ther*. 2006;5(12): 3162–3169.
27. Madhankumar AB, Slagle-Webb B, Wang X, et al. Efficacy of interleukin-13 receptor-targeted liposomal doxorubicin in the intracranial brain tumor model. *Mol Cancer Ther*. 2009;8(3):648–654.
28. Nguyen V, Conyers JM, Zhu D, et al. IL-13Ralpha2-Targeted Therapy Escapees: Biologic and Therapeutic Implications. *Transl Oncol*. 2011;4(6):390–400.
29. Chittiboina P, Heiss JD, Warren KE, Lonser RR. Magnetic resonance imaging properties of convective delivery in diffuse intrinsic pontine gliomas. *J Neurosurg Pediatr*. 2014;13(3):276–282.
30. Debinski W, Miner R, Leland P, Obiri NI, Puri RK. Receptor for interleukin (IL) 13 does not interact with IL4 but receptor for IL4 interacts with IL13 on human glioma cells. *J Biol Chem*. 1996;271(37):22428–22433.
31. Lathia JD, Gallagher J, Heddleston JM, et al. Integrin alpha 6 regulates glioblastoma stem cells. *Cell Stem Cell*. 2010;6(5): 421–432.
32. Hernandez-Caselles T, Villalain J, Gomez-Fernandez JC. Stability of liposomes on long term storage. *J Pharm Pharmacol*. 1990;42(6): 397–400.
33. Corathers SD. Focus on diagnosis: the alkaline phosphatase level: nuances of a familiar test. *Pediatr Rev*. 2006;27(10):382–384.
34. Allhenn D, Shetab Boushehri MA, Lamprecht A. Drug delivery strategies for the treatment of malignant gliomas. *Int J Pharm*. 2012;436(1-2):299–310.
35. Ding D, Kanaly CW, Bigner DD, et al. Convection-enhanced delivery of free gadolinium with the recombinant immunotoxin MR1–1. *J Neurooncol*. 2010;98(1):1–7.
36. Salomir R, Hokland S, Pedersen M. Magnetic resonance imaging (MRI)-directed focussed [*sic*] ultrasound. Methods and applications in oncological treatment [Article in Danish]. *Ugeskr Laeger*. 2005;167(39):3667–3672.
37. Treat LH, McDannold N, Vykhodtseva N, Zhang Y, Tam K, Hynynen K. Targeted delivery of doxorubicin to the rat brain at therapeutic levels using MRI-guided focused ultrasound. *Int J Cancer*. 2007; 121(4):901–907.
38. Yowell SL, Blackwell S. Novel effects with polyethylene glycol modified pharmaceuticals. *Cancer Treat Rev*. 2002;28 (Suppl A): 3–6.
39. Ng K, Zhao L, Liu Y, Mahapatro M. The effects of polyethyleneglycol (PEG)-derived lipid on the activity of target-sensitive immunoliposome. *Int J Pharm*. 2000;193(2):157–166.
40. Immordino ML, Dosio F, Cattel L. Stealth liposomes: review of the basic science, rationale, and clinical applications, existing and potential. *Int J Nanomedicine*. 2006;1(3):297–315.
41. Perche F, Torchilin VP. Recent trends in multifunctional liposomal nanocarriers for enhanced tumor targeting. *J Drug Deliv*. 2013;1: 1–32.
42. Bedu-Addo FK, Tang P, Xu Y, Huang L. Effects of polyethyleneglycol chain length and phospholipid acyl chain composition on the interaction of polyethyleneglycol-phospholipid conjugates with phospholipid: implications in liposomal drug delivery. *Pharm Res*. 1996;13(5):710–717.
43. Haar PJ, Broaddus WC, Chen ZJ, Fatouros PP, Gillies GT, Corwin FD. Gd-DTPA T1 relaxivity in brain tissue obtained by convection-enhanced delivery, magnetic resonance imaging and emission spectroscopy. *Phys Med Biol*. 2010;55(12): 3451–3465.